Supplementary Information (SI) for Nanoscale.

ELECTRONIC SUPPLEMENTARY INFORMATION

Colloidal Gold-Palladium-Platinum Alloy Nanospheres with Tunable Compositions and Defined Number of Atoms

Sergio Triviño-Sánchez,[a] Ren Xu, [a] Jesús González-Izquierdo, [a] Luis Bañares, [a] Israel Cano, [b] Jorge Pérez-Juste, [c] Andrés Guerrero-Martínez* [a] and Guillermo González-Rubio*[a]

[a] *Departamento de Química Física, Universidad Complutense de Madrid, 28040 Madrid, Spain.*
[b] *Departamento de Química Inorgánica, Universidad Complutense de Madrid, 28040 Madrid, Spain.*
[c] *Departamento de Química Física, Universidad de Vigo, 36310 Vigo, Spain.*

*Corresponding authors´ e-mail: aguerrero@quim.ucm.es, ggrubio@ucm.es

Table S1. Experimental feeding ratios employed for the synthesis of the different bimetallic and trimetallic heterostructures

NCs	$[Au^0]$ (M)	$[Pd^{2+}]$	$[Pd^0]$	$[Pt^{2+}]$
$Au_7@Pd_{93}$ NCs	0.03	0.4		
$Au_{10}@Pd_{90}$ NCs	0.044	0.4		
$Au_{18}@Pd_{82}$ NCs	0.087	0.4		
$Au_7@Pd_{63}@Pt_{30}$ NCs	0.093		0.83	0.4
$Au_7@Pd_{33}@Pt_{60}$ NCs	0.046		0.22	0.4
$Au_7@Pt_{93}$ NCs	0.03			0.4

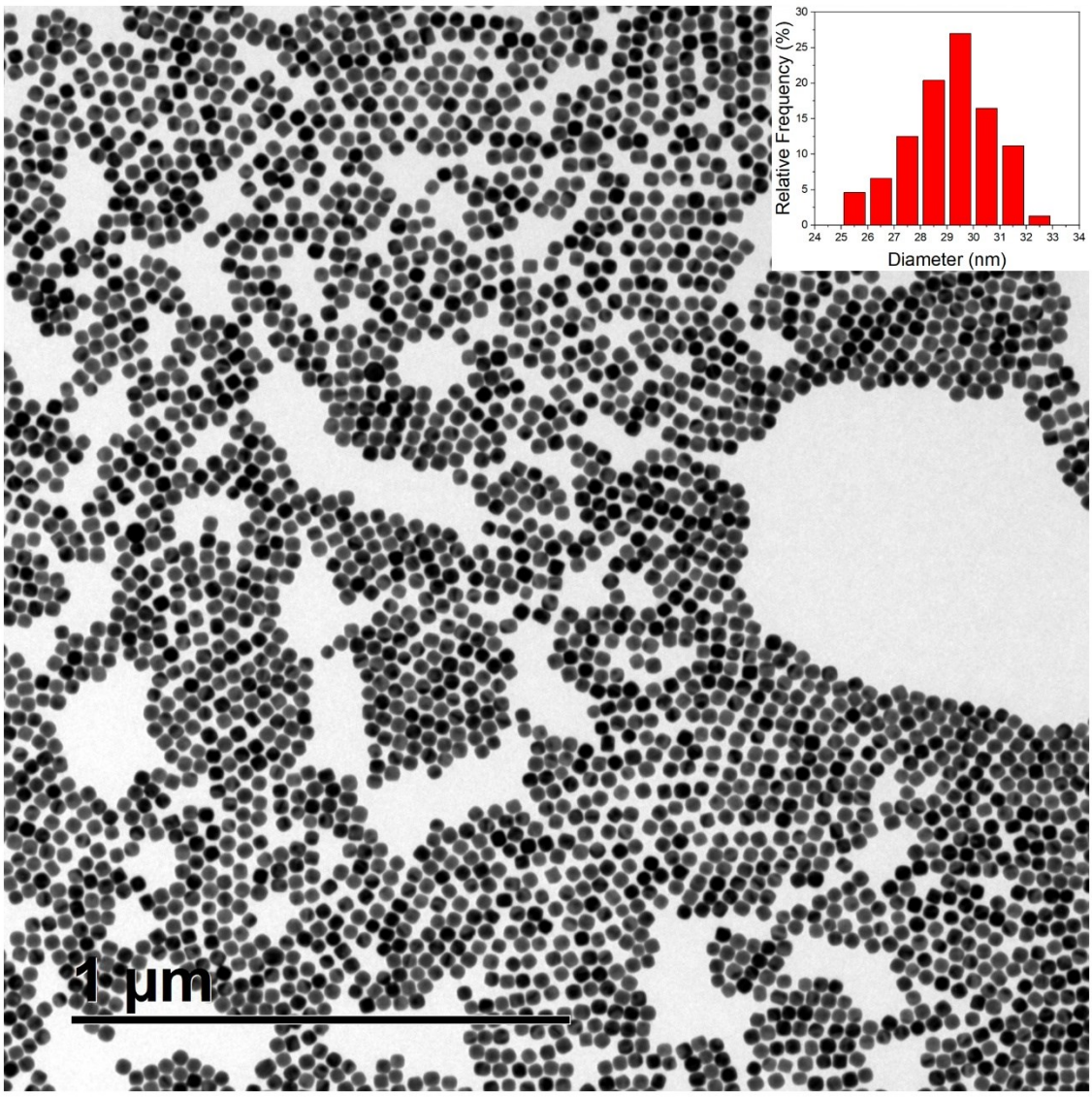

Fig. S1. Low-magnification TEM image of 30 nm Au NCs used as seeds for the growth of Au@Pt, Au@Pd and Au@Pd@Pt NCs and the corresponding size distribution histogram (inset).

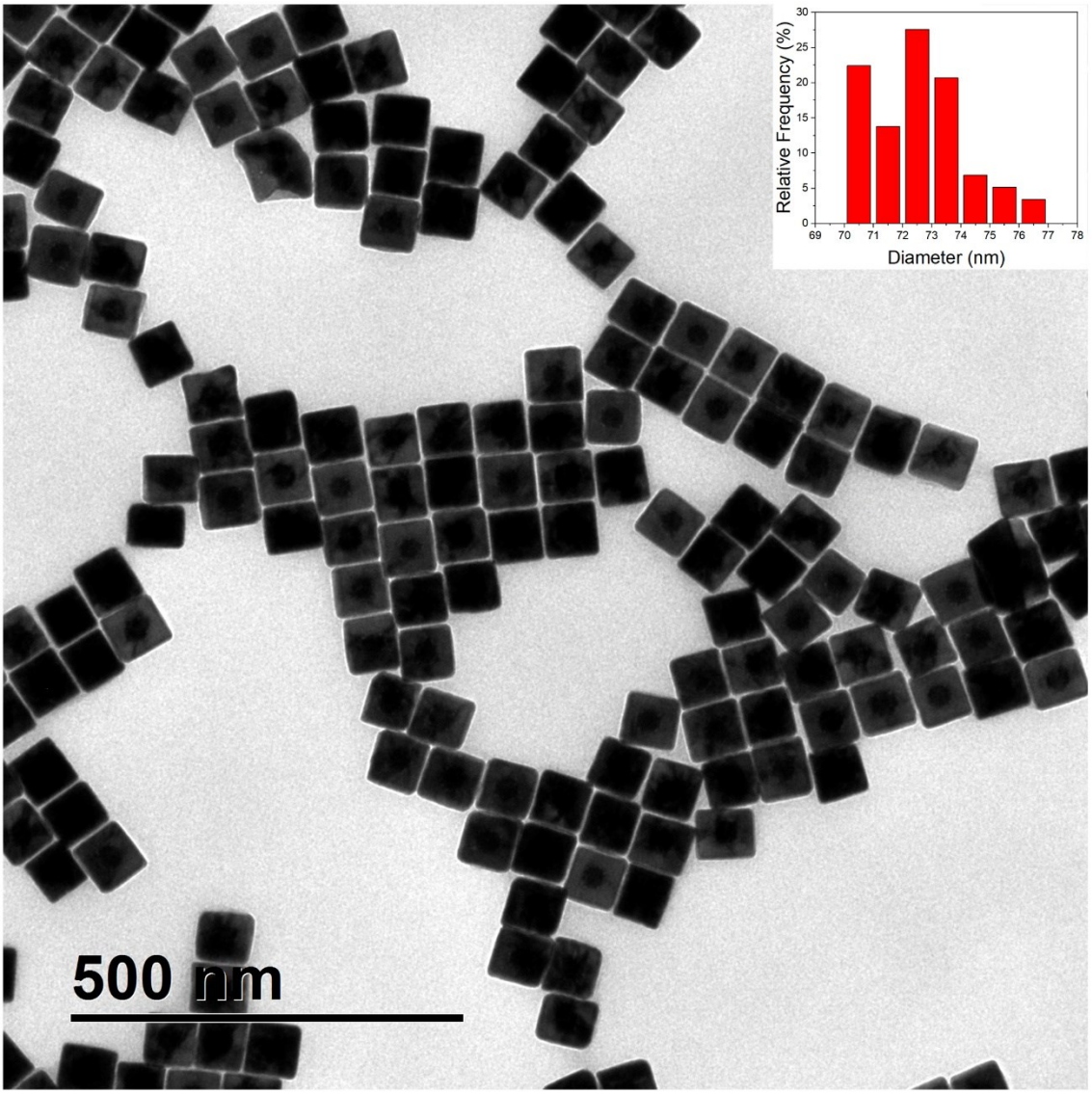

Fig. S2. Low-magnification TEM image of $Au_7@Pd_{93}$ NCs and the corresponding size distribution histogram (inset). .

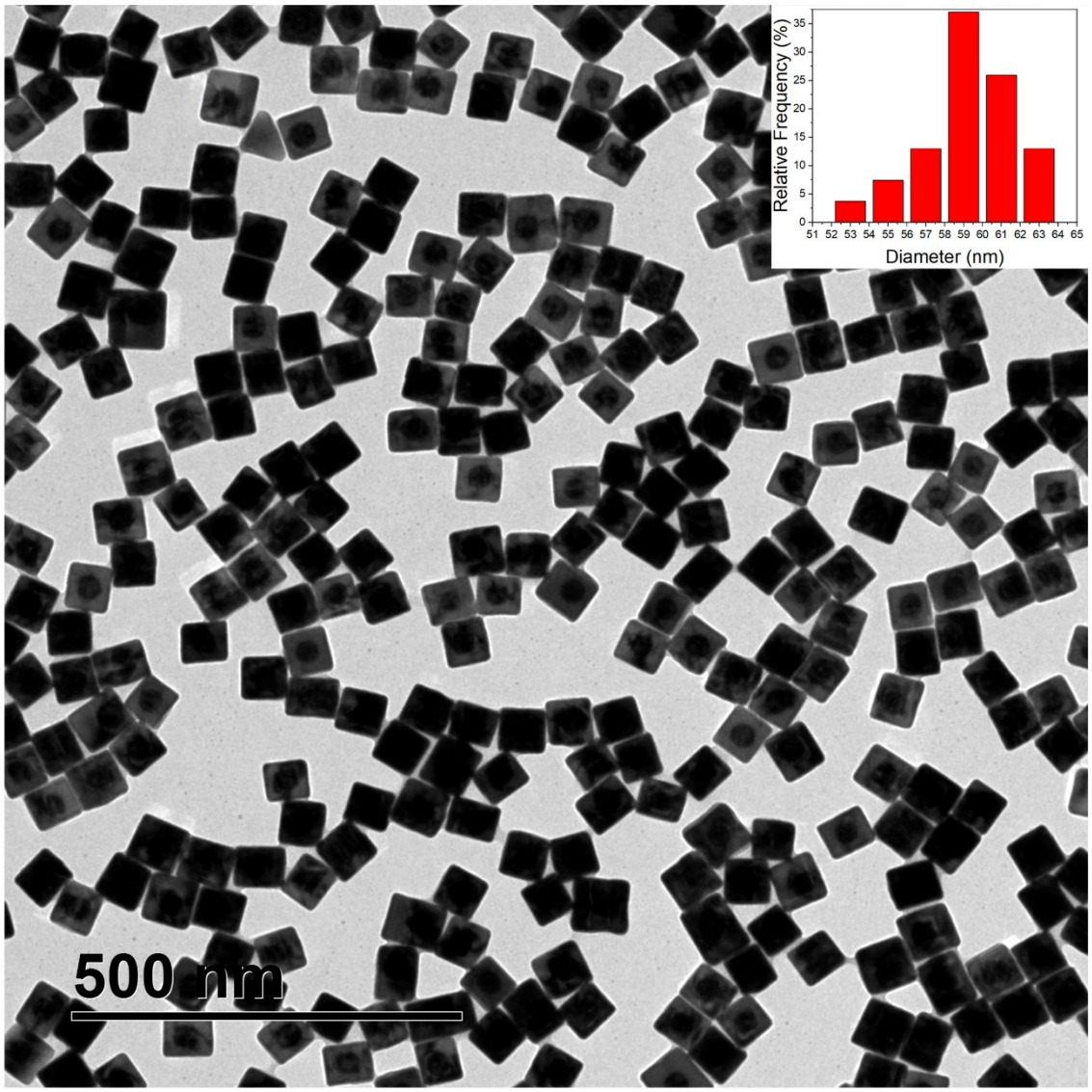

Fig. S3. Low-magnification TEM image of $Au_{10}@Pd_{90}$ NCs and the corresponding size distribution histogram (inset). .

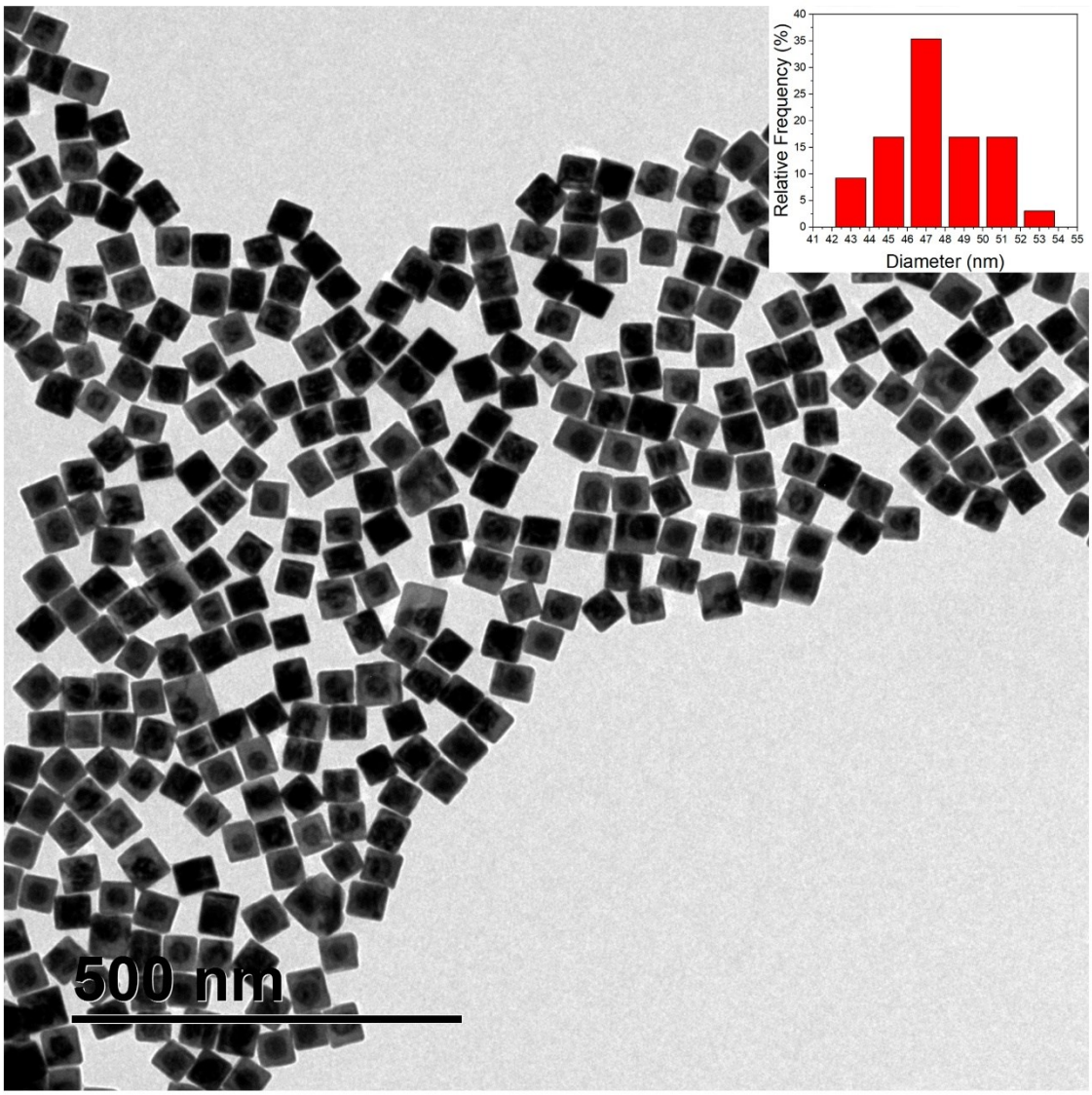

Fig. S4. Low-magnification TEM image of Au_{18}@Pd_{82} NCs and the corresponding size distribution histogram (inset). .

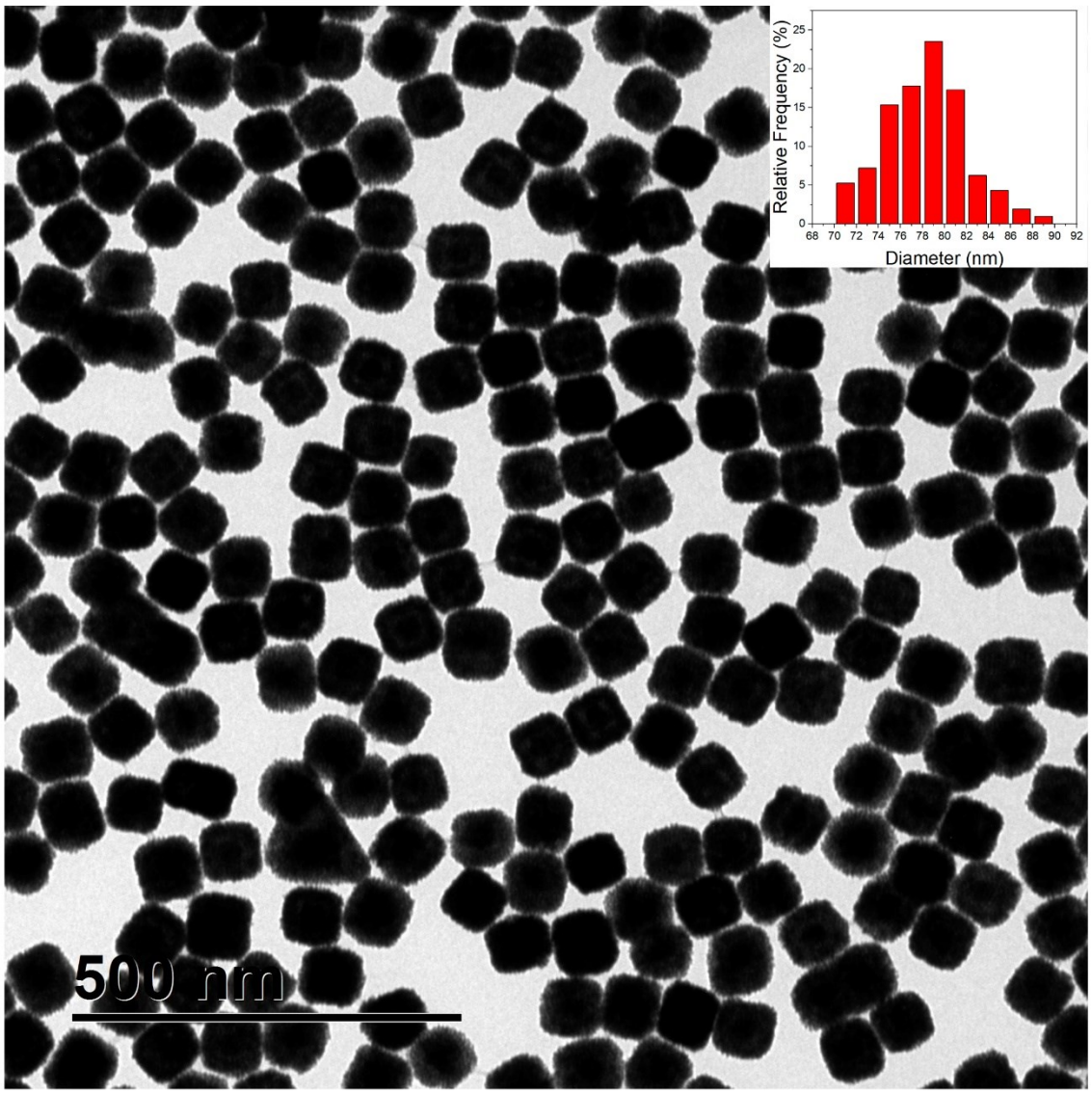

Fig. S5. Low-magnification TEM image of $Au_7@Pd_{33}@Pt_{60}$ NCs and the corresponding size distribution histogram (inset). .

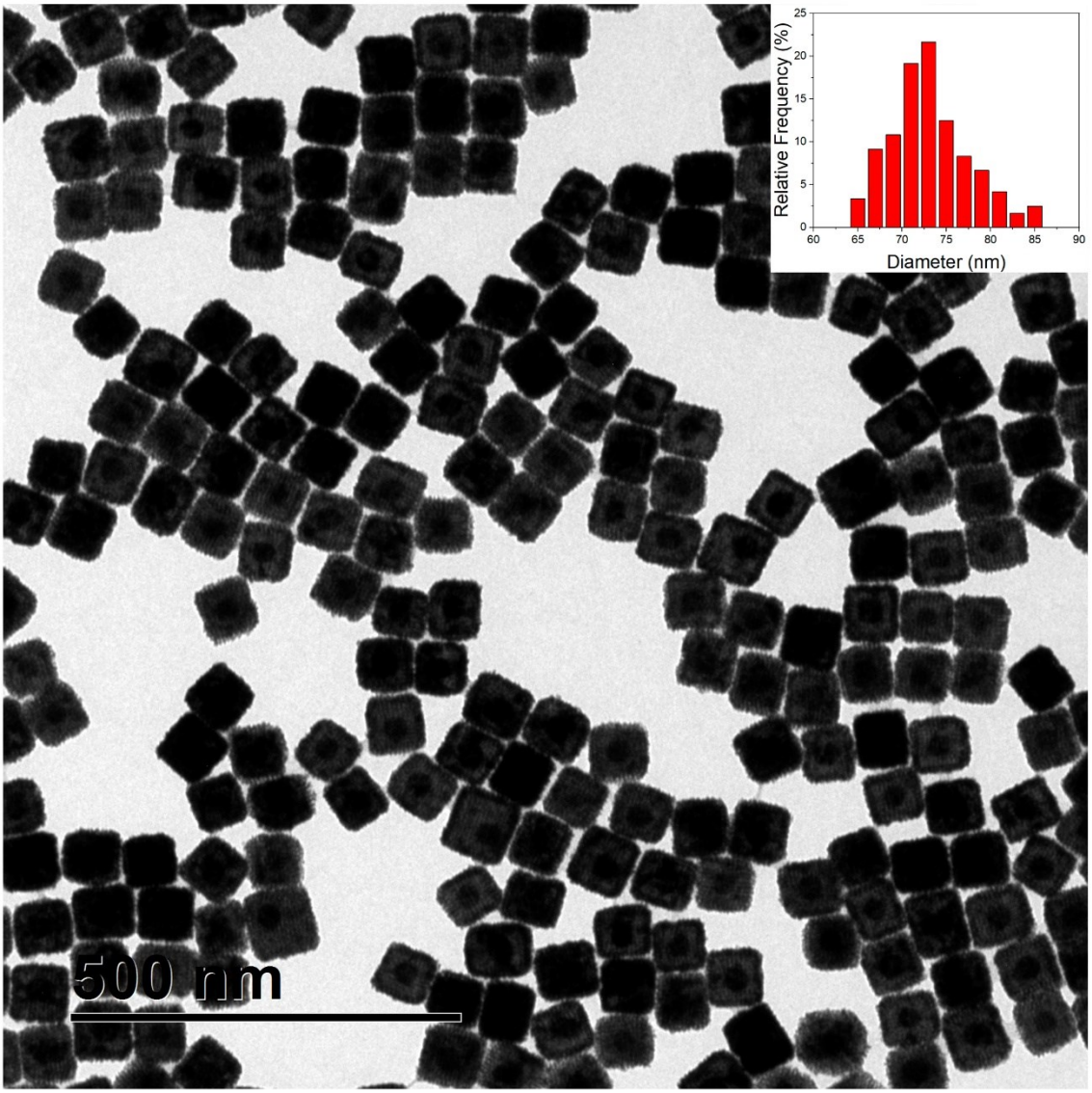

Fig. S6. Low-magnification TEM image of $Au_7@Pd_{63}@Pt_{30}$ NCs and the corresponding size distribution histogram (inset). .

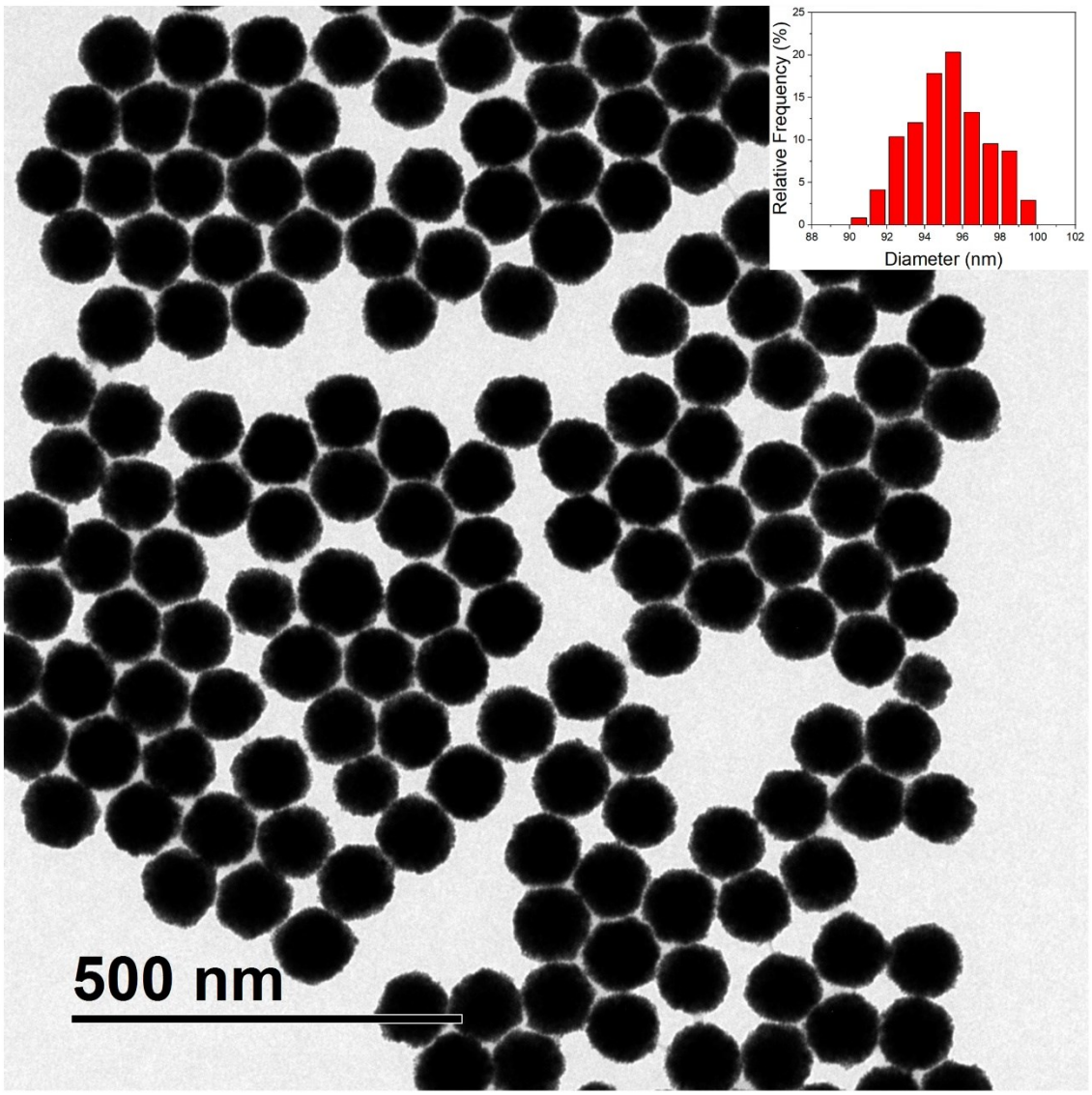

Fig. S7. Low-magnification TEM image of $Au_7@Pt_{93}$ NCs and the corresponding size distribution histogram (inset). .

Table S2. Elemental atomic composition of the synthesized heterostructure and alloy NCs determined through EDX spectroscopy.

NCs	Au %	Pd %	Pt %
$Au_7@Pd_{93}$ NCs	7.5 ± 0.7	92.5 ± 0.7	
Au_7Pd_{93} NCs	5.3 ± 0.2	94.7 ± 0.2	
$Au_7@Pd_{63}@Pt_{30}$ NCs	6.9 ± 0.5	64 ± 1	29 ± 1
$Au_7Pd_{63}Pt_{30}$ NCs	5.2 ± 0.3	58.5 ± 0.3	36.3 ± 0.3
$Au_7@Pd_{33}@Pt_{60}$ NCs	7.5 ± 0.3	33.5 ± 0.9	59.0 ± 0.8
$Au_7Pd_{33}Pt_{60}$ NCs	4.4 ± 0.2	27.8 ± 0.9	67.8 ± 0.9
$Au_7@Pt_{93}$ NCs	8.1 ± 0.8		91.9 ± 0.8
Au_7Pt_{93} NCs	7 ± 1		93 ± 1

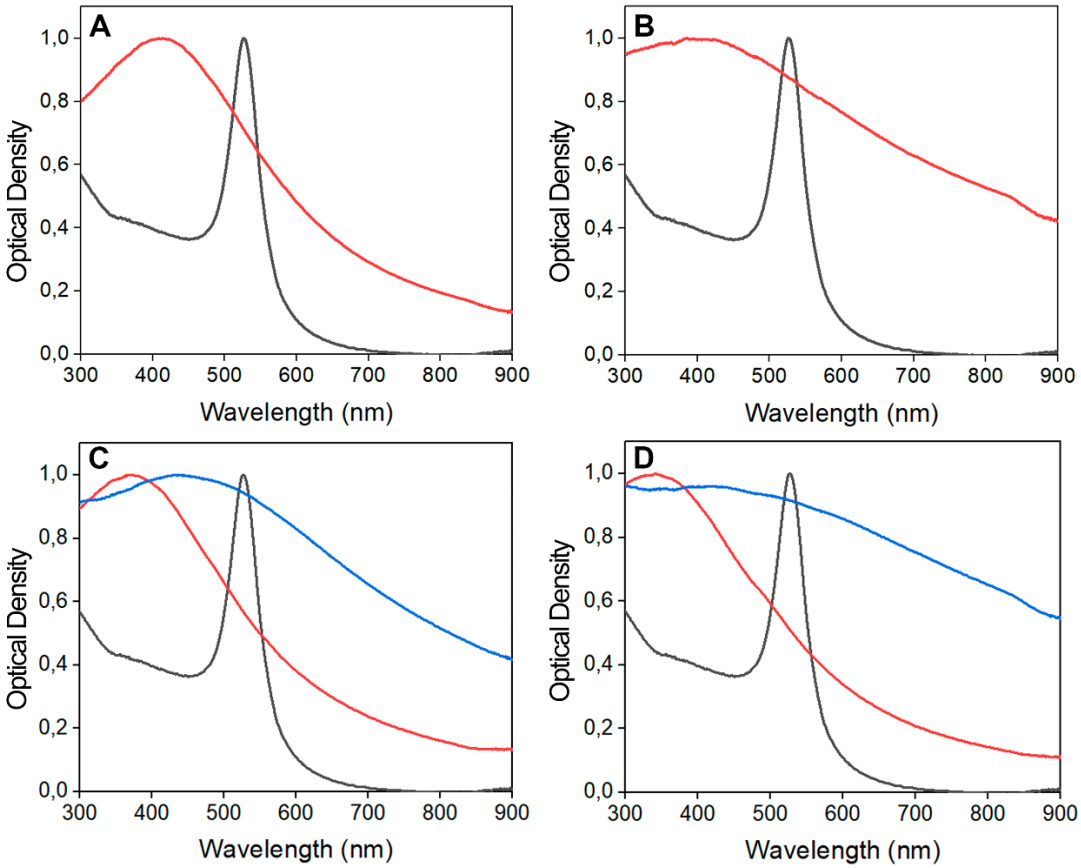

Fig. S8. Normalized UV-Vis-NIR spectra of Au NCs (black, A-D), $Au_7@Pd_{93}$ NCs (red, A), $Au_7@Pt_{93}$ NCs (red, B), $Au_{10}@Pd_{90}$ NCs (red, C) and $Au_7@Pd_{63}@Pt_{30}$ NCs (blue, C), $Au_{18}@Pd_{82}$ NCs (red, D) and $Au_7@Pd_{33}@Pt_{60}$ NCs (blue, D).

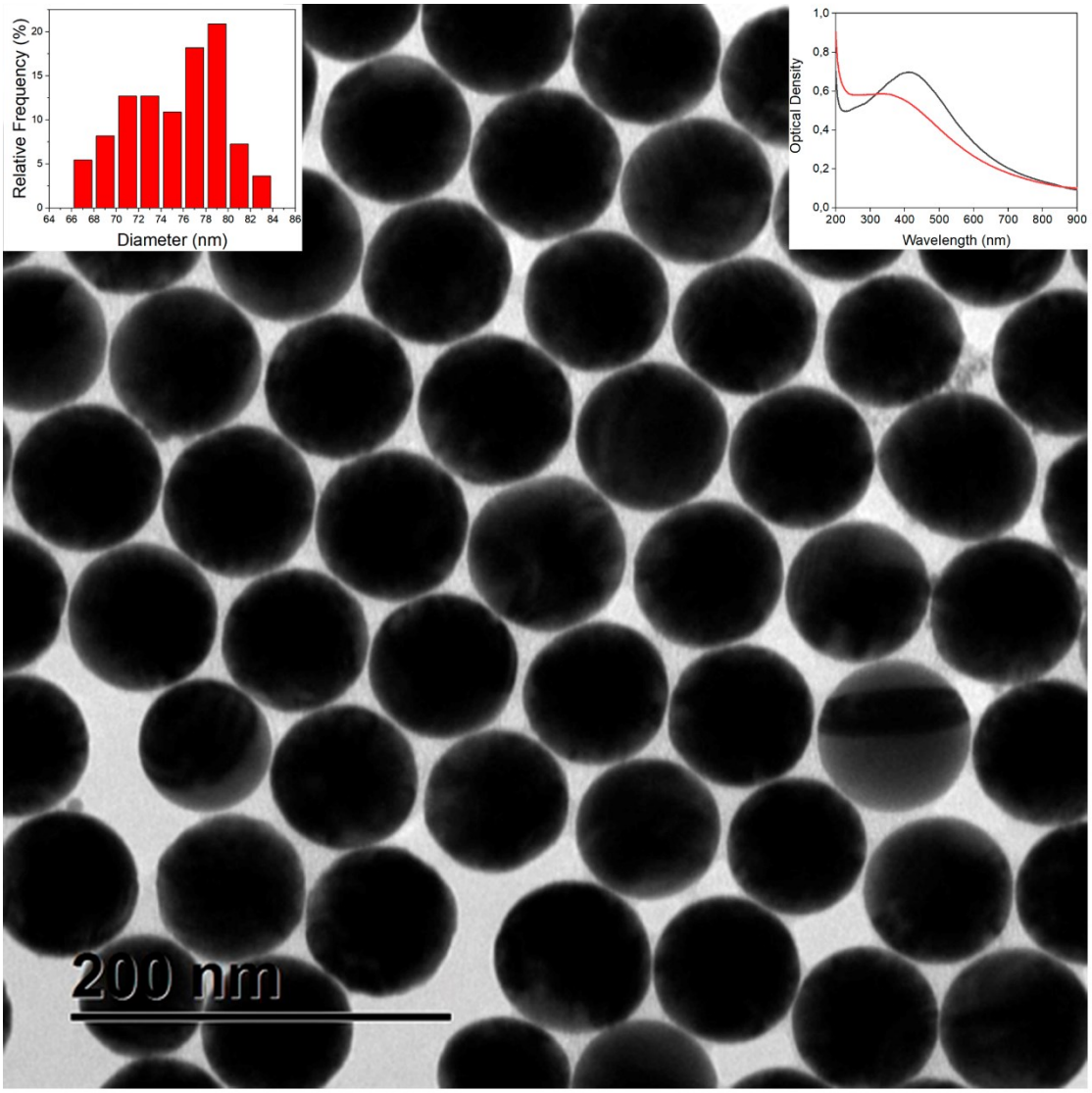

Fig. S9. Low-magnification TEM image, size distribution histogram (left inset) and UV-Vis-NIR spectra of Au_7Pd_{93} NCs (right inset, red) synthesized *via* irradiation of $Au_7@Pd_{93}$ NCs with ns-pulsed laser irradiation (right inset, black).

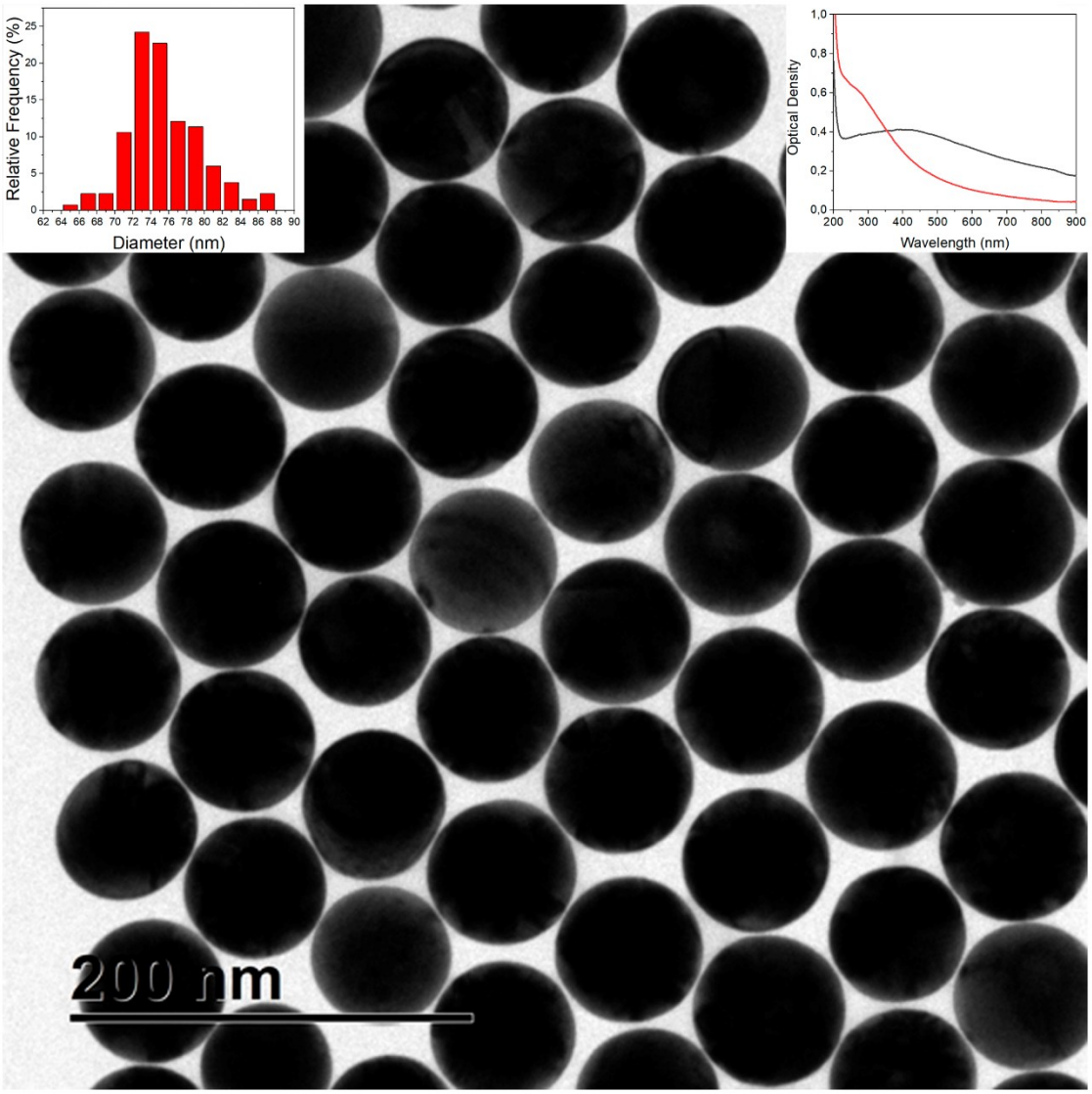

Fig. S10. Low-magnification TEM image, size distribution histogram (left inset) and UV-Vis-NIR spectra of Au_7Pt_{93} NCs (right inset, red) synthesized *via* irradiation of $Au_7@Pt_{93}$ NCs with ns-pulsed laser irradiation (right inset, black).

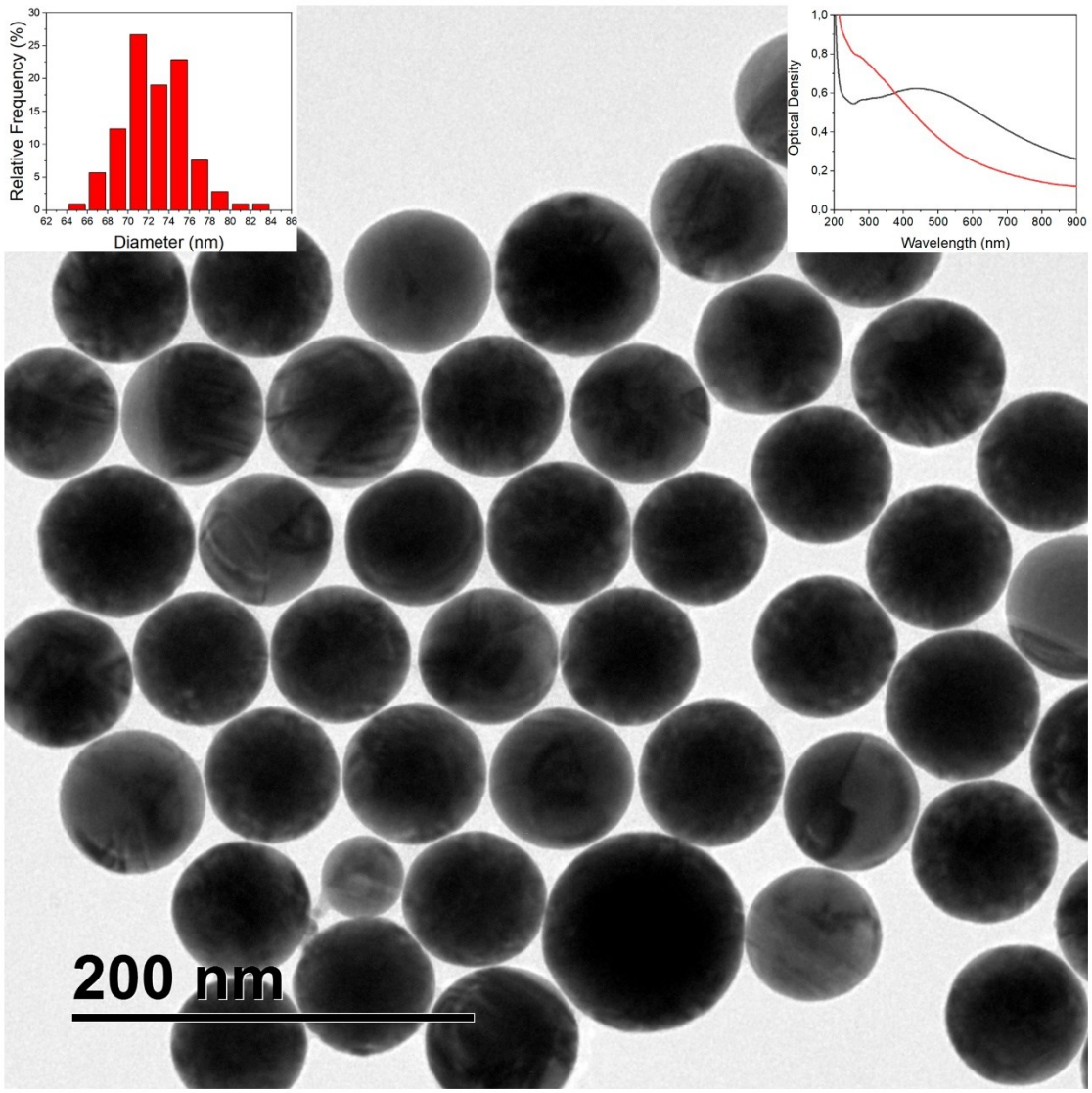

Fig. S11. Low-magnification TEM image, size distribution histogram (left inset) and UV-Vis-NIR spectra of $Au_7Pd_{63}Pt_{30}$ NCs (right inset, red) synthesized *via* irradiation of $Au_7@Pd_{63}@Pt_{30}$ NCs with ns-pulsed laser irradiation (right inset, black).

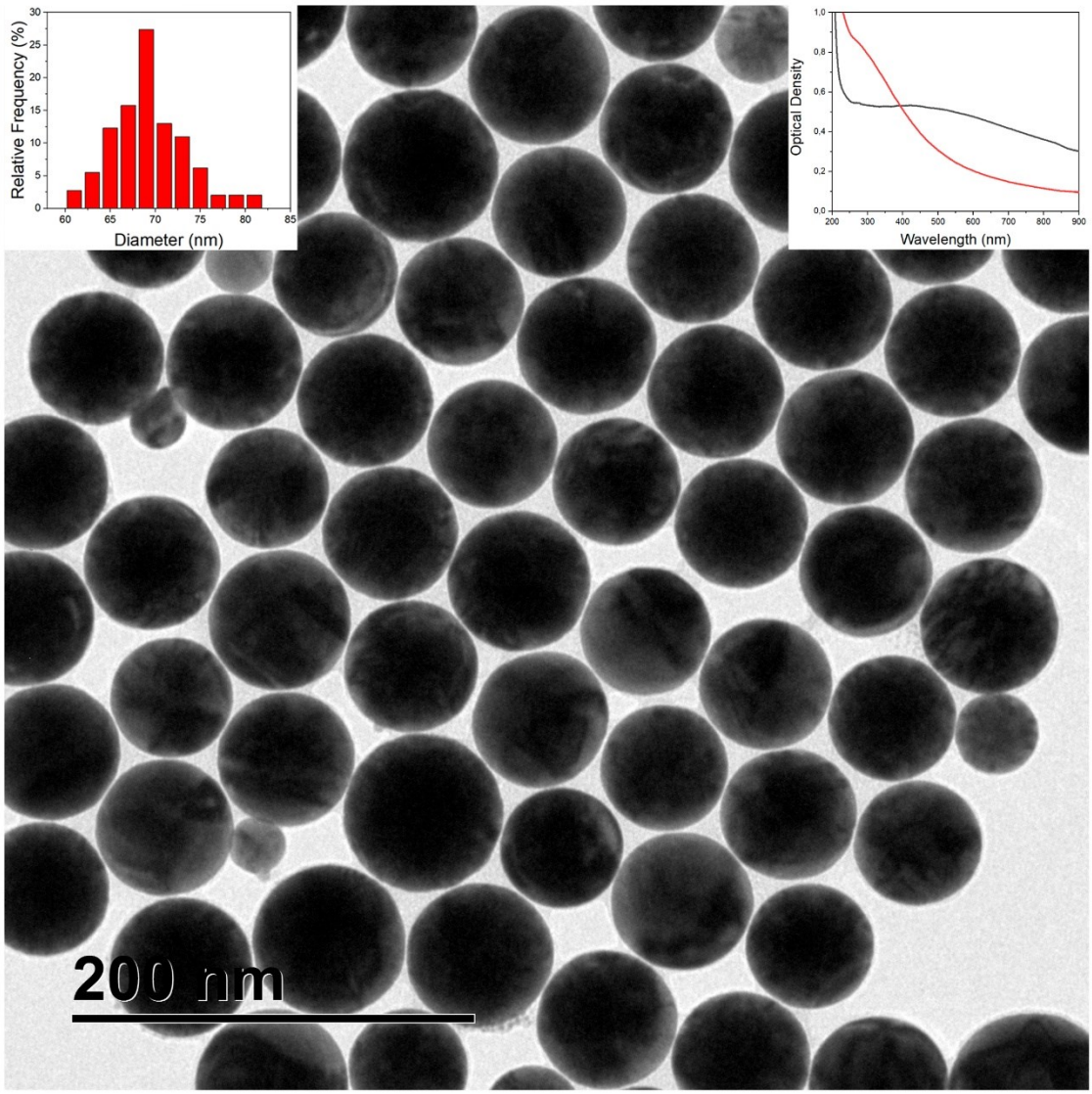

Fig. S12. Low-magnification TEM image, size distribution histogram (left inset) and UV-Vis-NIR spectra of $Au_7Pd_{33}Pt_{60}$ NCs (right, red) synthesized *via* irradiation of $Au_7@Pd_{33}@Pt_{60}$ NCs with ns-pulsed laser irradiation (right inset, black).

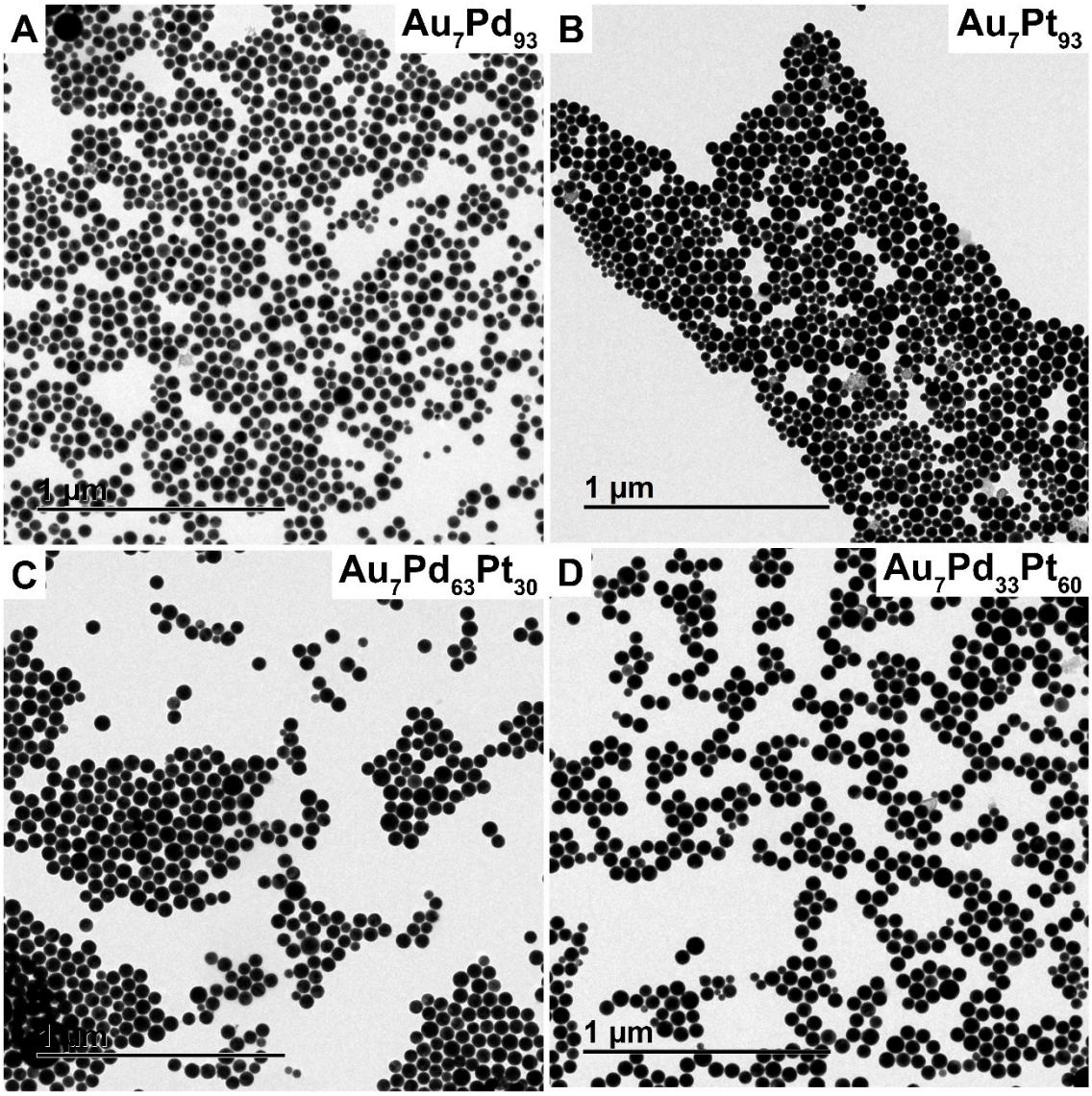

Fig. S13. Low-magnification TEM images of Au_7Pd_{93} NCs (A), Au_7Pt_{93} NCs (B), $Au_7Pd_{63}Pt_{30}$ NCs (C) and $Au_7Pd_{33}Pt_{60}$ NCs (D) irradiated at a high fluence (96 J/m^2), for which fragmentation of the excited NCs occurred.

.

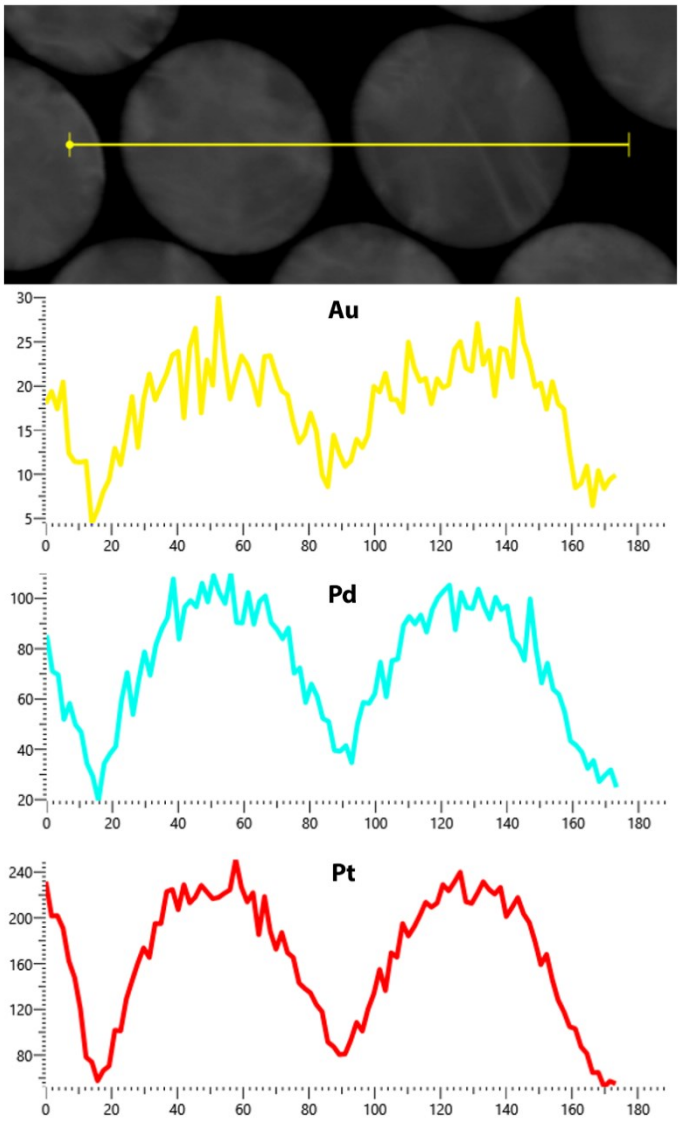

Fig. S14. Elemental distribution by EDX line scan through the centre of the reconstructed of two $Au_7Pd_{33}Pt_{60}$ NCs.

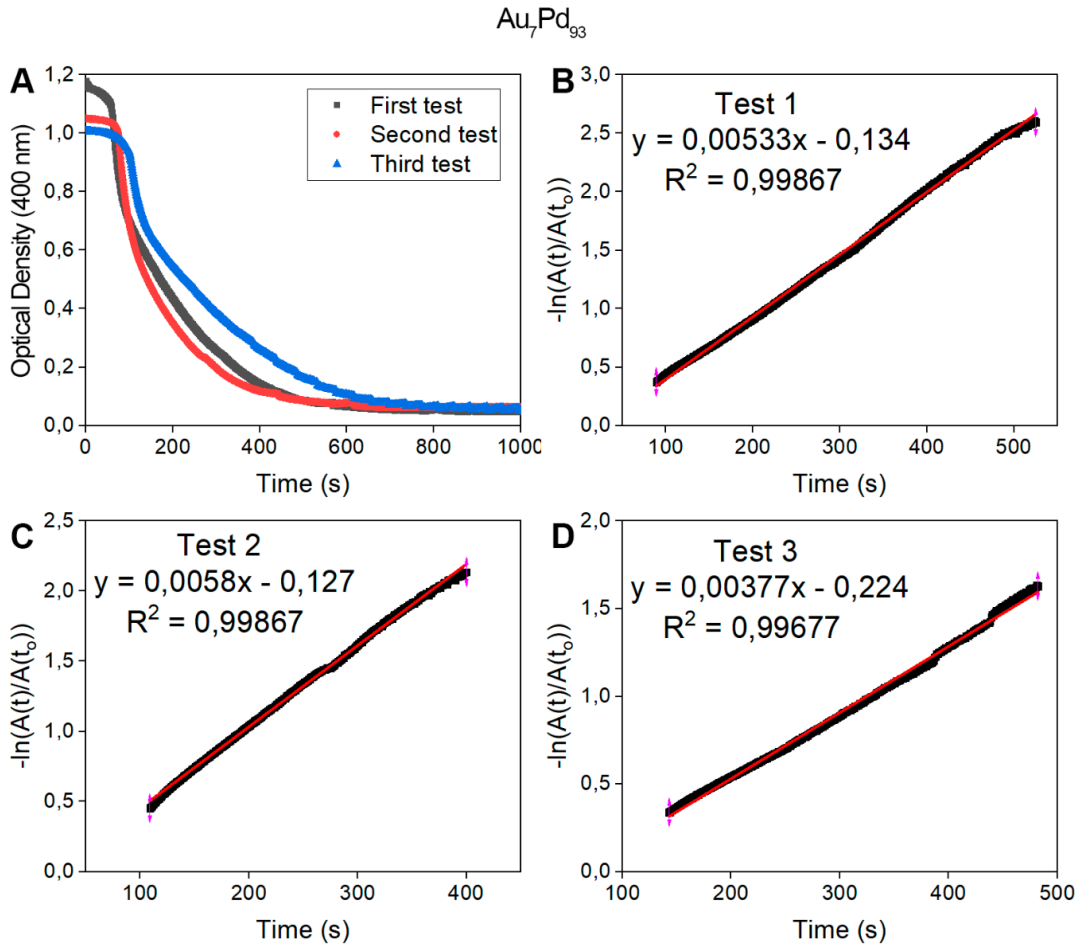

Fig. S15. (A) Time-dependence evolution of 4-nitrophenol absorbance at 400 nm during the reduction process catalysed by Au_7Pd_{93} NCs, where the graphs represent a series of experiments performed to investigate the reproducibility and reliability of the obtained results ([$NaBH_4$] = 80 mM). (B-D) The $-\ln(A(t)/A(t_0))$ vs. time plot (black) derived from the adjacent absorbance data and the fitted curve (red) from which k_{app} is extracted.

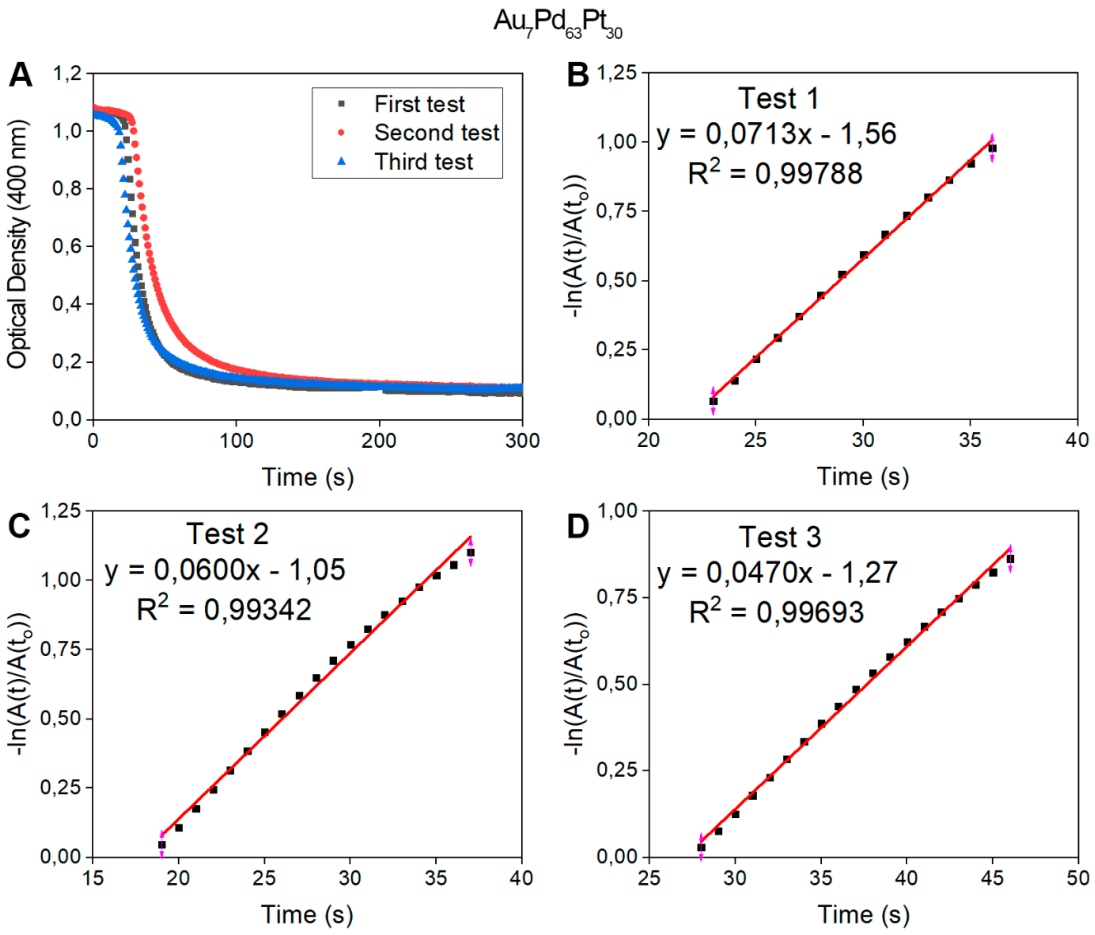

Fig. S16. (A) Time-dependence evolution of 4-nitrophenol absorbance at 400 nm during the reduction process catalysed by $Au_7Pd_{63}Pt_{30}$ NCs, where the graphs represent a series of experiments performed to investigate the reproducibility and reliability of the obtained results ([$NaBH_4$] = 80 mM). (B-D) The $-\ln(A(t)/A(t_0))$ vs. time plot (black) derived from the adjacent absorbance data and the fitted curve (red) from which k_{app} is extracted.

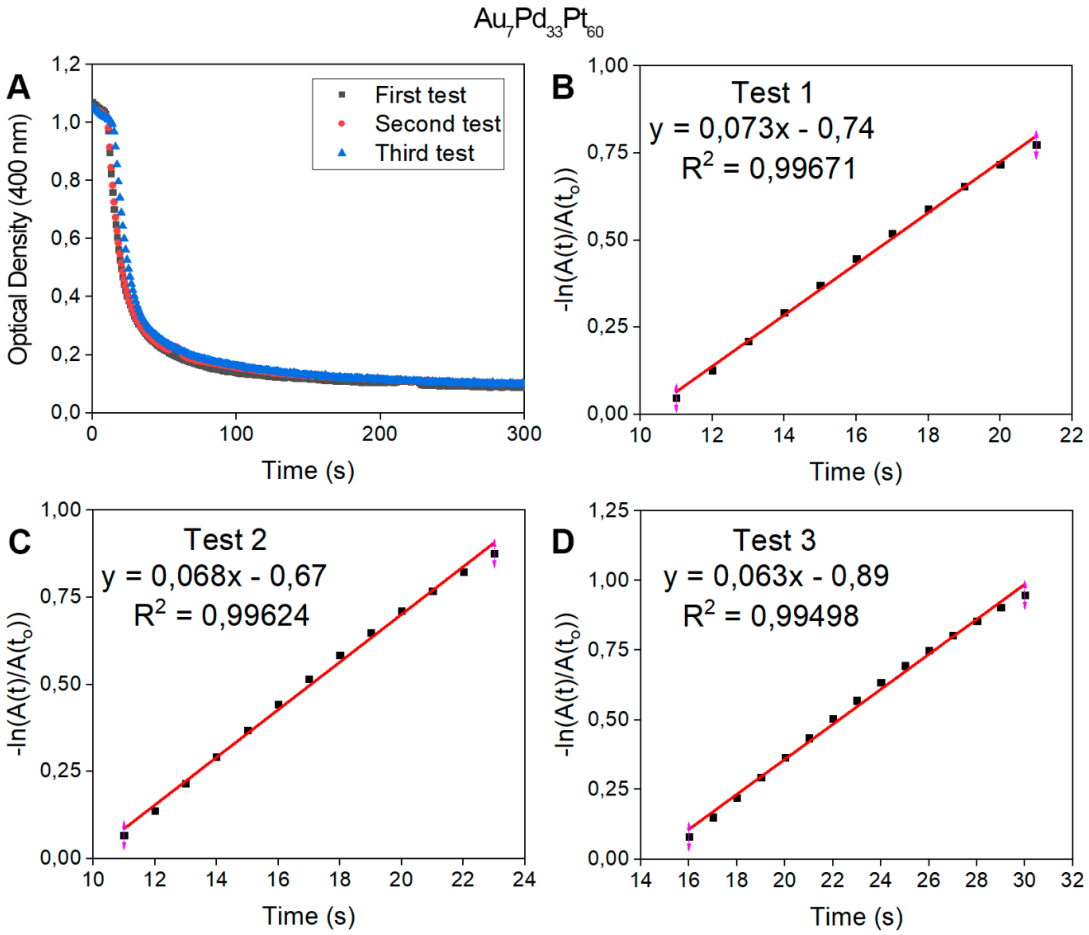

Fig. S17. (A) Time-dependence evolution of 4-nitrophenol absorbance at 400 nm during the reduction process catalysed by $Au_7Pd_{33}Pt_{60}$ NCs, where the graphs represent a series of experiments performed to investigate the reproducibility and reliability of the obtained results ([$NaBH_4$] = 80 mM). (B-D) The $-\ln(A(t)/A(t_0))$ vs. time plot (black) derived from the adjacent absorbance data and the fitted curve (red) from which k_{app} is extracted.

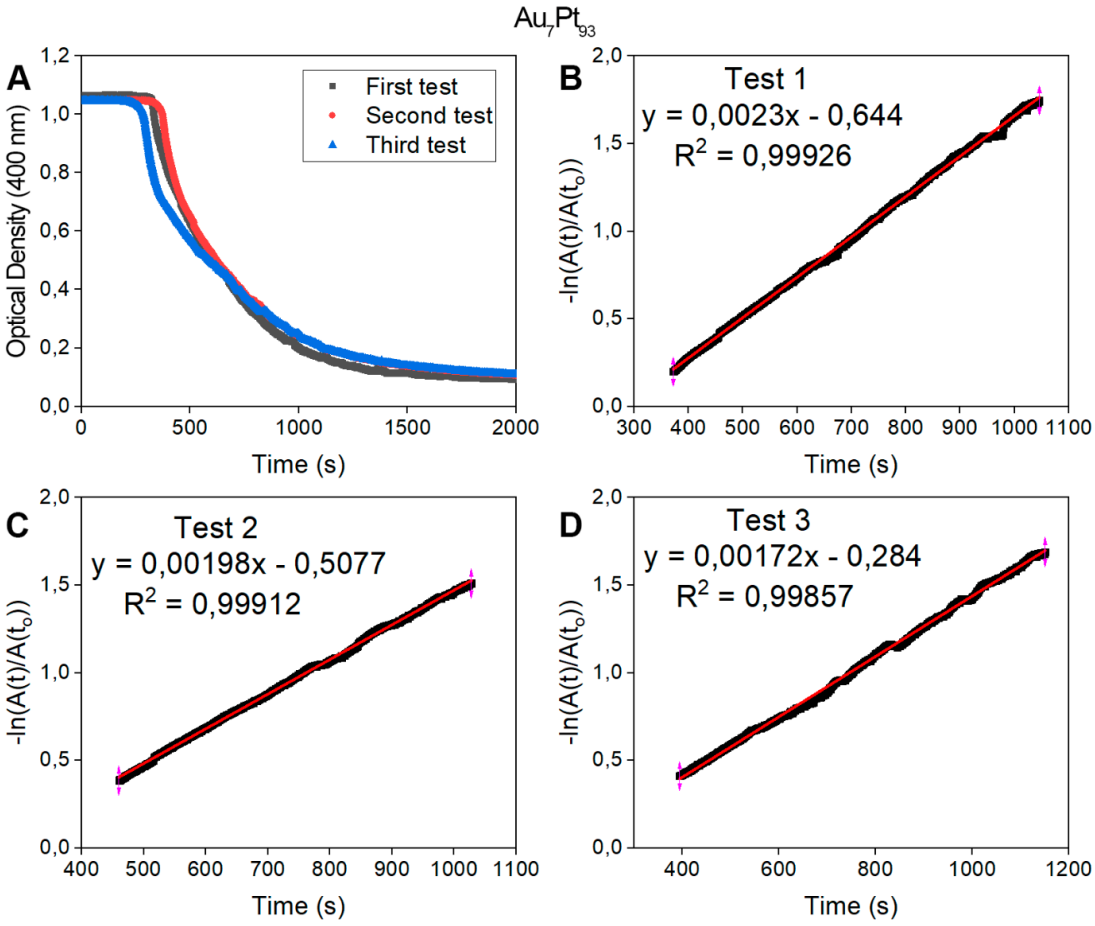

Fig. S18. (A) Time-dependence evolution of 4-nitrophenol absorbance at 400 nm during the reduction process catalysed by Au_7Pt_{93} NCs, where the graphs represent a series of experiments performed to investigate the reproducibility and reliability of the obtained results ([$NaBH_4$] = 80 mM). (B-D) The $-\ln(A(t)/A(t_0))$ vs. time plot (black) derived from the adjacent absorbance data and the fitted curve (red) from which k_{app} is extracted.

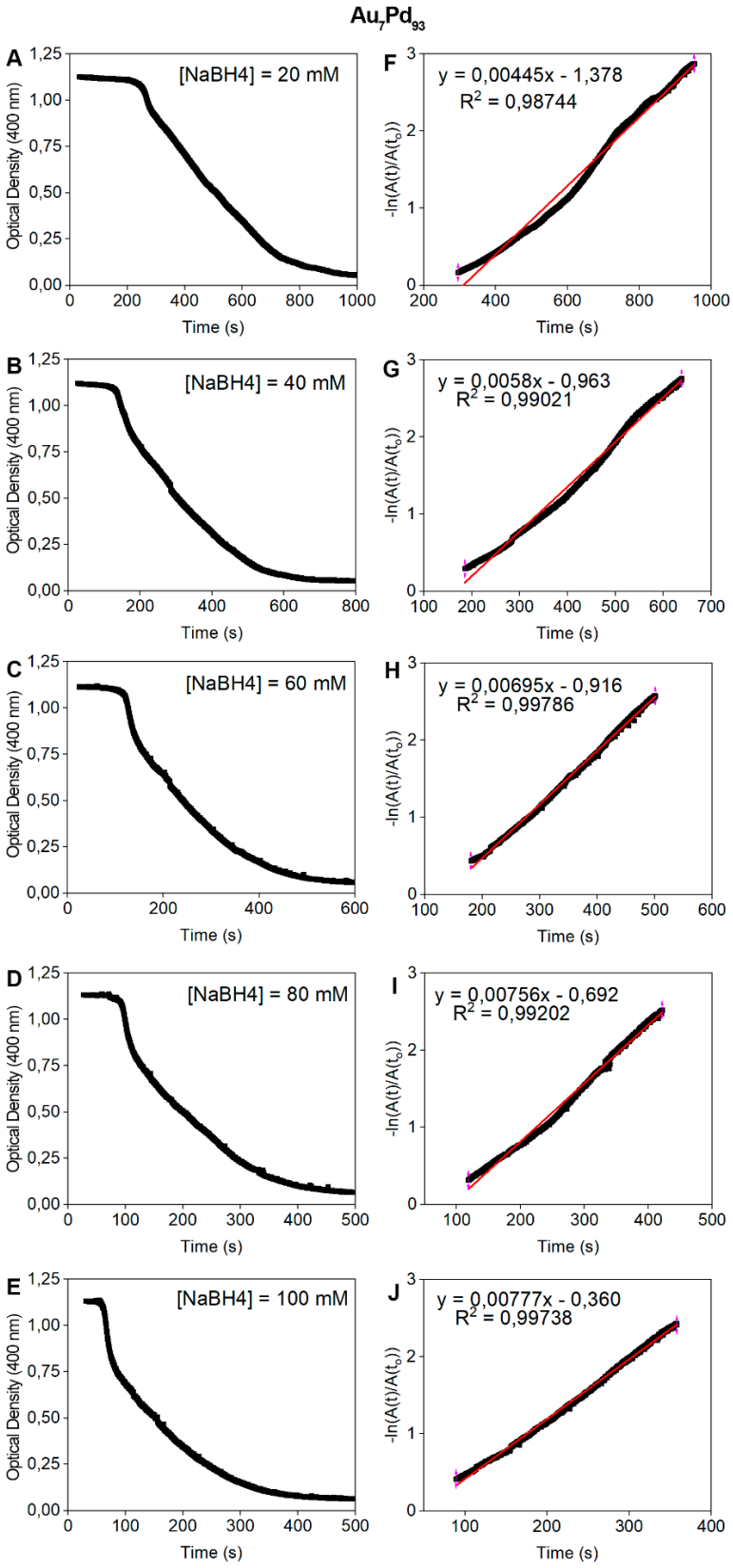

Fig. S19. (A–E) Time-dependence evolution of 4-nitrophenol absorbance at 400 nm during the reduction process catalysed by Au_7Pd_{93} NCs, where each graph represents a different concentration of $NaBH_4$. (F–J) The $-\ln(A(t)/A(t_0))$ vs. time plot (black) derived from the adjacent absorbance data and the fitted curve (red) from which k_{app} is extracted.

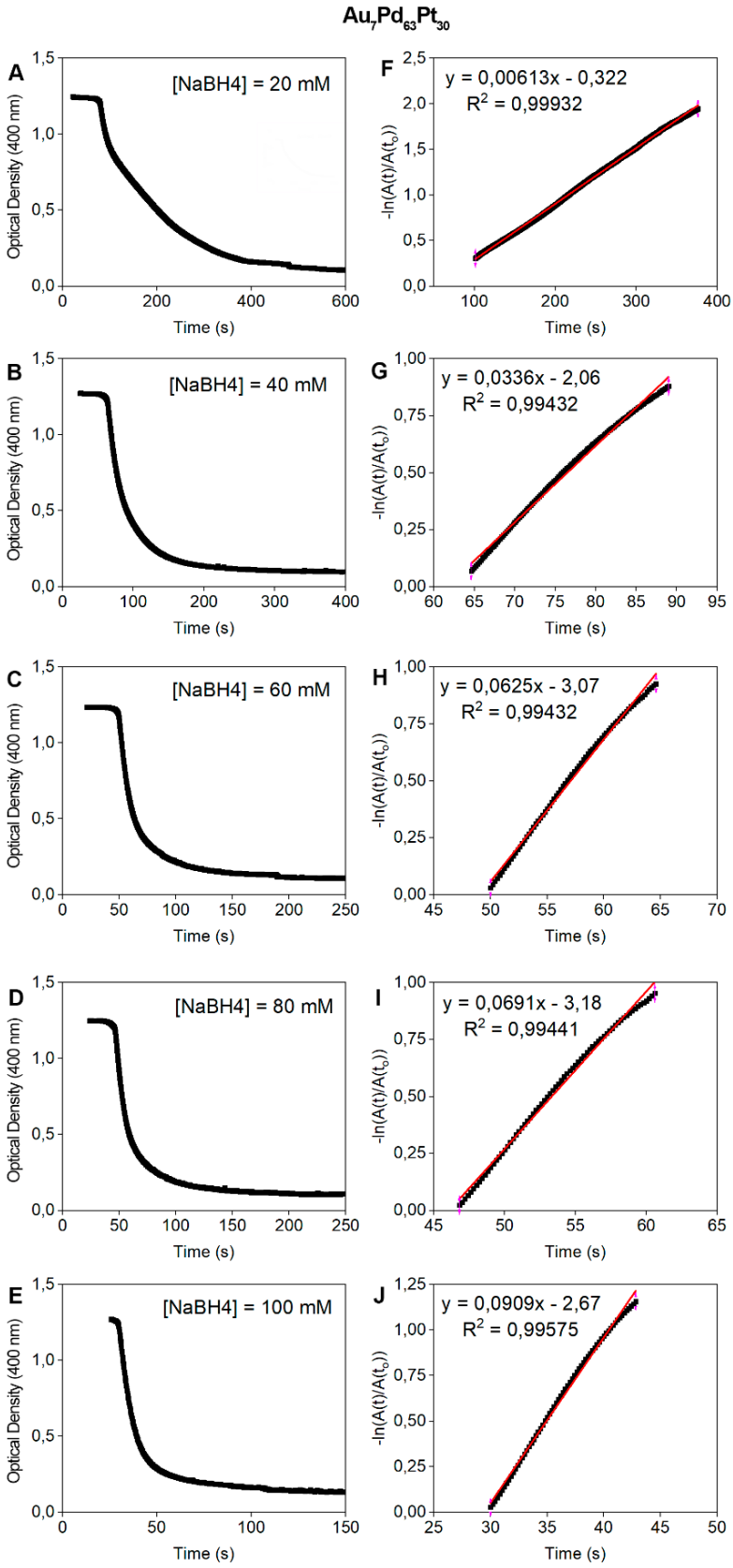

Fig. S20. (A–E) Time-dependence evolution of 4-nitrophenol absorbance at 400 nm during the reduction process catalysed by $Au_7Pd_{63}Pt_{30}$ NCs, where each graph represents a different concentration of $NaBH_4$. (F–J) The $-\ln(A(t)/A(t_0))$ vs. time plot (black) derived from the adjacent absorbance data and the fitted curve (red) from which k_{app} is extracted.

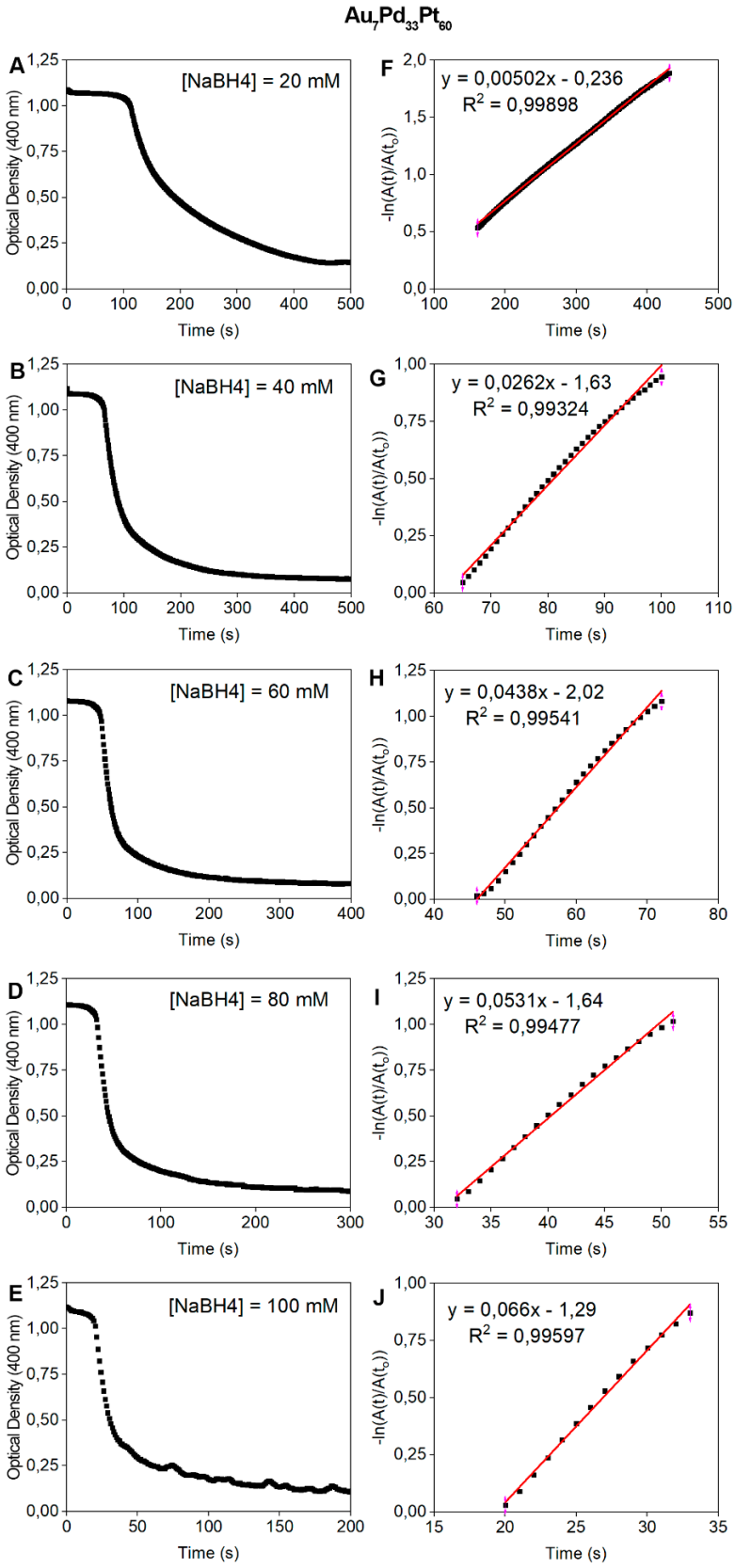

Fig. S21. (A–E) Time-dependence evolution of 4-nitrophenol absorbance at 400 nm during the reduction process catalysed by $Au_7Pd_{33}Pt_{60}$ NCs, where each graph represents a different concentration of $NaBH_4$. (F–J) The $-\ln(A(t)/A(t_0))$ vs. time plot (black) derived from the adjacent absorbance data and the fitted curve (red) from which k_{app} is extracted.

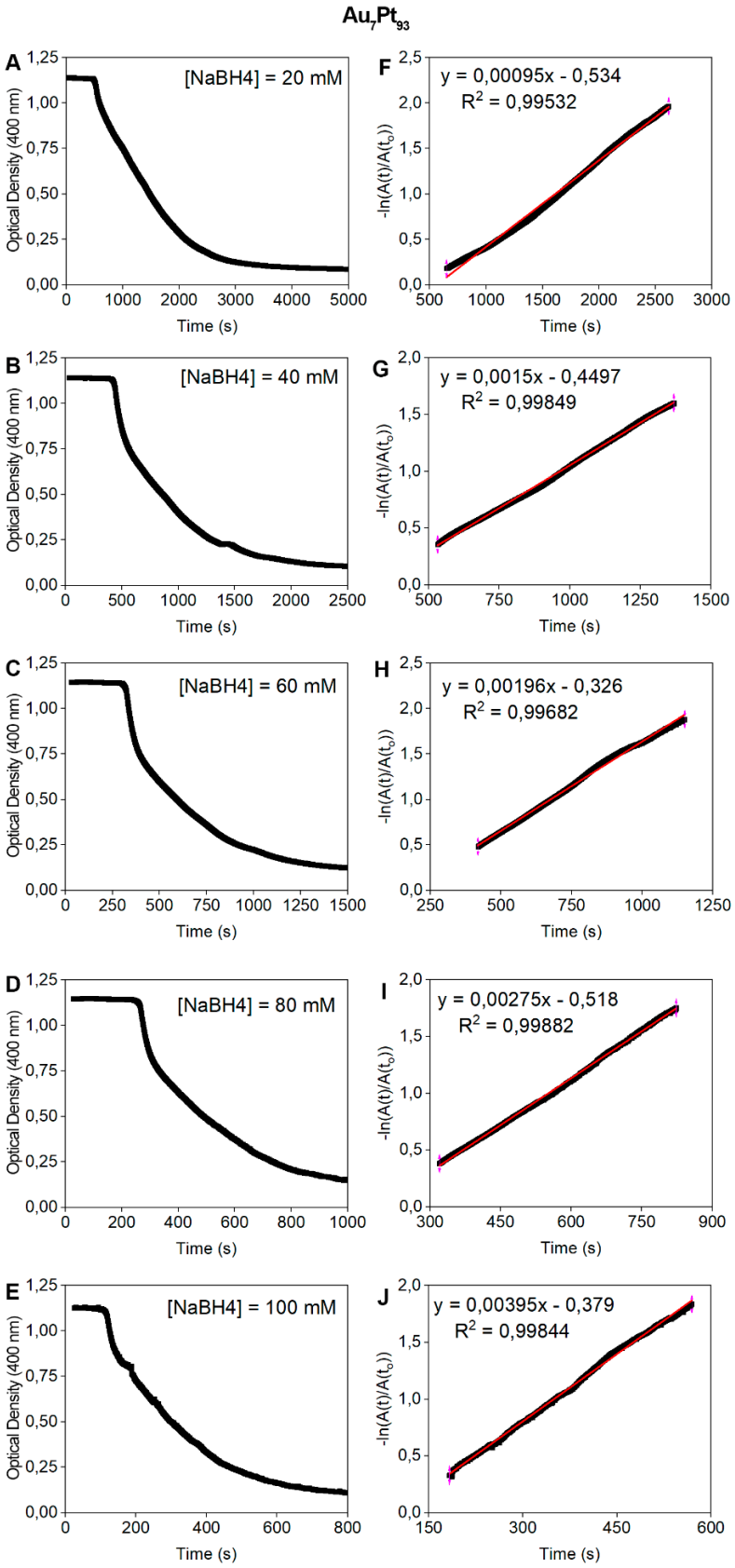

Fig. S22. (A–E) Time-dependence evolution of 4-nitrophenol absorbance at 400 nm during the reduction process catalysed by Au_7Pt_{93} NCs, where each graph represents a different concentration of $NaBH_4$. (F–J) The $-\ln(A(t)/A(t_0))$ vs. time plot (black) derived from the adjacent absorbance data and the fitted curve (red) from which k_{app} is extracted.

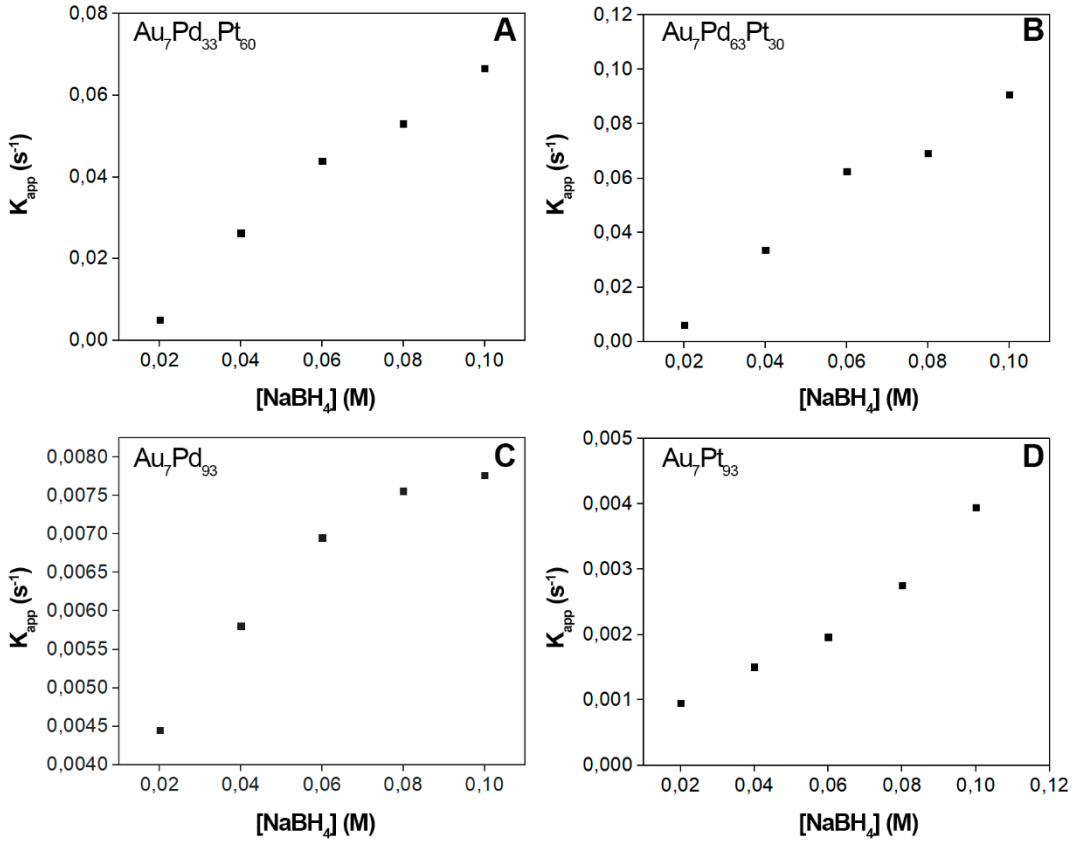

Fig. S23. Variation of k_{app} with the concentration of sodium borohydride for the catalytic reduction of 4-nitrophenol using $Au_7Pd_{33}Pt_{60}$ NCs (A), $Au_7Pd_{63}Pt_{30}$ NCs (B), Au_7Pd_{93} NCs (C) and Au_7Pt_{93} NCs (D) as catalysts. A linear variation of k_{app} can be noticed in the 20-100 mM range in all cases, except for that of Au_7Pd_{93} NCs, which occurs in the 20-80 mM range. These results indicate that the concentration of sodium borohydride utilized in this work (80 mM) is sufficiently high to consider the validity of the pseudo-first-order reaction assumption.

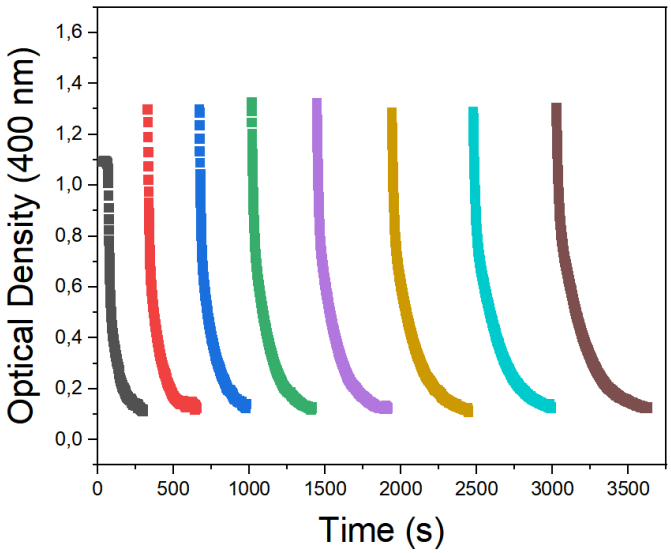

Fig. S24. Optical density kinetic traces at 400 nm recorded during the sequential reduction of 4-nitrophenol through the addition of 58 mM nitrophenol after each catalytic cycle in the presence of 80 mM $NaBH_4$. Each addition is marked with distinct colours, grey: first, red: second, blue: third, green: fourth, purple: fifth, yellow: sixth, cyan: seventh and brown: eighth. The determined k_{norm} were*:* 8.4 10^6, 7 10^6, 6.2 10^6, 4.2 10^6, 3.8 10^6, 3.7 10^6, 3.7 10^6, 3.7 10^6 $mol^{-1} \cdot s^{-1} \cdot M^{-1}$, respectively.